Mass Spectrometry

International Edition: DOI: 10.1002/anie.201607003
German Edition: DOI: 10.1002/ange.201607003

Multidimensional Mass Spectrometry of Synthetic Polymers and Advanced Materials**

*Chrys Wesdemiotis**

ion mobility · LC-MS · mass spectrometry · polymers · tandem MS

Multidimensional mass spectrometry interfaces a suitable ionization technique and mass analysis (MS) with fragmentation by tandem mass spectrometry (MS^2) and an orthogonal online separation method. Separation choices include liquid chromatography (LC) and ion-mobility spectrometry (IMS), in which separation takes place pre-ionization in the solution state or post-ionization in the gas phase, respectively. The MS step provides elemental composition information, while MS^2 exploits differences in the bond stabilities of a polymer, yielding connectivity and sequence information. LC conditions can be tuned to separate by polarity, end-group functionality, or hydrodynamic volume, whereas IMS adds selectivity by macromolecular shape and architecture. This Minireview discusses how selected combinations of the MS, MS^2, LC, and IMS dimensions can be applied, together with the appropriate ionization method, to determine the constituents, structures, end groups, sequences, and architectures of a wide variety of homo- and copolymeric materials, including multicomponent blends, supramolecular assemblies, novel hybrid materials, and large cross-linked or nonionizable polymers.

1. Introduction

Mass spectrometry (MS) has become an essential analytical tool in polymer and materials science, in which it is increasingly used to verify or ascertain the microstructure of a wide range of synthetic polymers.[1–5] More widespread applications, similar to those in the -omics areas of biology and medicine,[6–8] are however hampered by the following limitations: 1) The sample must be capable of forming stable gas-phase ions, which precludes the analysis of saturated and very large or cross-linked polymers; 2) MS does not reveal specific information about the functional groups present in a polymeric material or about its primary and higher-order structure; and 3) mixtures and blends may not be characterized properly due to differences in ionization and detection efficiencies of their constituents. This Minireview discusses new developments that help to resolve these problems and broaden the utility of MS in polymer and materials science.

Chemical analysis by MS involves the conversion of the analyte molecules to gas-phase ions and the subsequent separation and detection of these ions according to their mass-to-charge ratio (m/z). The most widely used ionization methods for synthetic polymers are matrix-assisted laser desorption ionization (MALDI),[9,10] electrospray ionization (ESI),[11] and atmospheric-pressure chemical ionization (APCI),[12] which ionize macromolecules by ion attachment (usually H^+, Na^+, or Ag^+) or ion removal (usually H^+ from acidic analytes). The m/z values of the resulting $[M+X]^+$ and $[M-H]^-$ quasimolecular ions reveal the corresponding macromolecular compositions. Because the ions are separated before detection, MS affords fractionation by mass, a particularly useful feature for synthetic polymers, which generally exhibit a distribution of molecular weights. This unique property permits characterization of individual oligomers (*n*-

[*] Prof. Dr. C. Wesdemiotis
Department of Chemistry, The University of Akron
Akron, OH 44325 (USA)
E-mail: wesdemiotis@uakron.edu

[**] A list of the abbreviations used is supplied in Section 6.

mers), instead of the average composition that is probed by most spectroscopic analytical methods.

The m/z information available through MS measurement is often sufficient to deduce a polymer's compositional heterogeneity as well as its total chain-end-group and other functionality distributions.[1–5] Minor products can be detected with exceptional sensitivity, as long as they differ in mass from the main product to be separated in the m/z dimension. Owing to these advantages, MS is increasingly used in polymer and materials science for establishing or confirming macromolecular structures, elucidating polymerization mechanisms, and assessing the commercial viability of polymers based on identified byproducts.[1,13–23]

The simple concept of mass-based analysis creates significant challenges, however (see above). Polymerizations often generate mixtures that are impossible to characterize by simple (that is, 1D) MS because of discrimination effects in the ionization or detection events. Connectivity (that is, sequence) information is not revealed by 1D MS. Isomeric architectures cannot be distinguished by m/z measurements and this problem also applies to isobaric polymer constituents with very small mass differences (ppm level or less). Finally, ESI can result in overlapping charge distributions, complicating mass determination and compositional assignments. As will be demonstrated herein, such problems can be overcome by using tandem (that is, 2D) mass spectrometry (MS^2) and/or by interfacing MS with an orthogonal separation step, either before ionization utilizing liquid chromatography (LC), or after ionization by ion-mobility mass spectrometry (IM-MS).[24–27] Combining this approach with thermal degradation further extends its applicability to large, cross-linked polymers that cannot be directly ionized.[28,29]

2. Tandem Mass Spectrometry (MS^2)

In MS^2 studies, mass analysis is performed twice. One oligomer ion among those formed in the ion source is mass-selected and its internal energy is raised to induce fragmentation;[30–33] common ion-activation methods are collisionally activated dissociation (CAD), electron-transfer or electron-capture dissociation (ETD or ECD, respectively), and photodissociation (PD).[34] A second stage of mass analysis follows to determine the m/z values of the fragment ions. MS^2 experiments reveal individual polymer end groups;[35–45] in contrast, the 1D MS spectrum provides insight about the sum of chain end substituents present in the oligomer, which may also contain partial or complete monomer unit(s). Additionally, MS^2 can be employed to analyze copolymer sequences[46–54] and to differentiate polymer architectures,[55–60] as will be illustrated with selected examples in Section 2.1 and 2.2.

Chrys Wesdemiotis completed his Ph.D. at Technische Universität Berlin with Helmut Schwarz (1979). After a postdoctoral fellowship with Fred W. McLafferty at Cornell University (1980) and military service in Greece (1981–1983), he returned to Cornell as senior research associate (1983–1989). In 1989, he joined the University of Akron, where he currently is Distinguished Professor of Chemistry, Polymer Science, and Integrated Bioscience. Research in the Wesdemiotis group focuses on the development and application of mass-spectrometry methods for the characterization of synthetic polymers, advanced materials, and polymer–biomolecule conjugates and interfaces.

2.1. Polymer End Groups and Architectures

Figure 1a shows the MALDI mass spectrum of an α,ω-divinyl functionalized polystyrene (PS) ionized by Ag^+ addition.[59] The m/z values of the $[M+Ag]^+$ ions observed confirm the expected repeat unit (104 Da) and the presence of end groups with a total mass of 186 Da. The separate α- and ω-chain-end substituents are dissected by MS^2. This is exemplified in Figure 1b by the MS^2 spectrum of the silverated 19-mer, which includes two fragment series in the

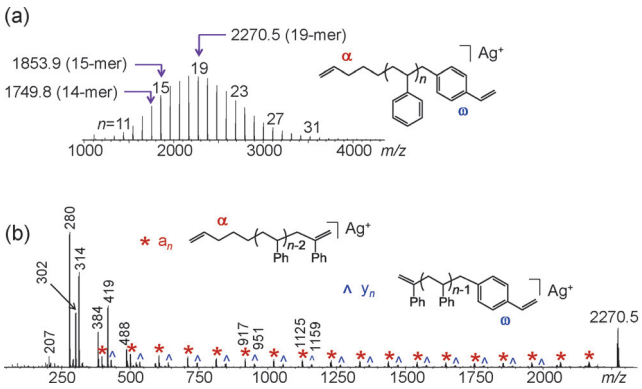

Figure 1. a) MALDI mass spectrum of α-4-pentenyl-ω-(*p*-vinylbenzyl)-polystyrene, acquired on a tandem time-of-flight (ToF/ToF) mass spectrometer; all ions are $[M+Ag]^+$ adducts. b) MALDI-MS^2 (CAD) spectrum of the $[M+Ag]^+$ ion from the 19-mer (m/z 2270.5); the fragments labeled by * and ^ contain the α and the ω end group, respectively. Adapted from Ref. [59] with permission.

medium- and high-mass range, one containing the α chain end (namely, a_n), and the other the ω chain end (namely, y_n).[33,37,38,59] These fragment series result from random homolytic backbone cleavages in the PS chain, followed by typical radical-induced decompositions, which coproduce radical ions and internal fragments in the low-mass range. The a_n and y_n series observed in the medium/high-mass range can be used to determine individual chain-end functionalities.

The fragment intensity pattern in the MS^2 spectrum of Figure 1b is diagnostic of a linear, chain-end-substituted architecture.[59,60] A dramatically different fragmentation pattern is observed for an in-chain-substituted or four-arm star-branched PS, as shown by the MS^2 spectra in Figure 2.[61,62] The in-chain-functionalized polymer (Figure 2a) produces approximately three Gaussian distributions of fragments with (b_{ni}) or without (b_n and a_n) the linking substituent and peaking at n of approximately 15–18, which is close to the average size of the PS chains used in the synthesis. This characteristic is caused by preferential bond breaking at or

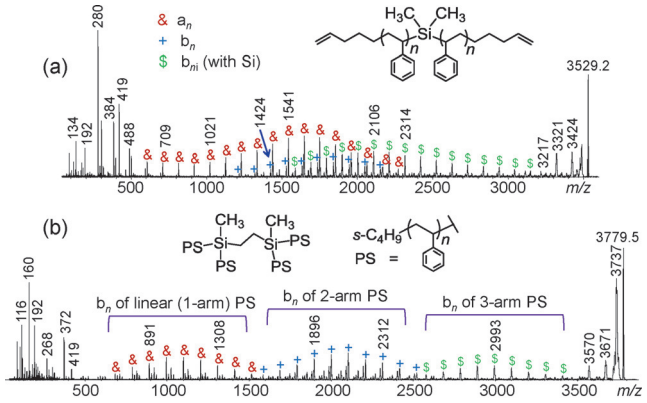

Figure 2. MALDI-MS^2 (CAD) spectra of the $[M+Ag]^+$ ions from a) the 31-mer of an in-chain-functionalized polystyrene and b) the 32-mer of a 4-arm star-branched polystyrene, acquired on a ToF/ToF mass spectrometer. The polymers were prepared by combining polystyryllithium with $(CH_3)_2SiCl_2$ and $Cl_2(CH_3)Si(CH_2)_2Si(CH_3)Cl_2$, respectively.[61,62] a) The a_n, b_n, and b_{ni} fragments carry a s-C_4H_9 group at one chain end; the other chain-end substituent is $CH_2CH(Ph)=CH_2$ for a_n, $CH=CH(Ph)$ for b_n and $Si(CH_3)_2C(Ph)=CH_2$ for b_{ni}. b) The 3-arm and 2-arm b_n fragments contain the $Si(CH_2)_2Si$ linker unit, a $CH=C(Ph)$ unit in one of their arms, and either one (3-arm b_n) or two Si–H (2-arm b_n) bonds. All a- and b-type fragments are ionized by Ag^+.

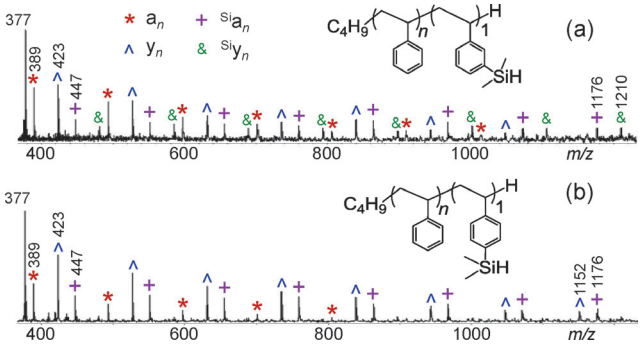

Figure 3. MALDI-MS^2 (CAD) spectra of the $[M+Li]^+$ ions from copolymers built from styrene and either *m*- or *p*-(dimethylsilyl)styrene, acquired on a ToF/ToF mass spectrometer. Very similar spectra are obtained for $n=11$–15; those shown were acquired from the most intense oligomers with a) $n=13$ (m/z 1580.0) and b) $n=15$ (m/z 1788.2). Adapted from Ref. [54] with permission.

near the linking substituent owing to steric crowding around the Si atom and silicon's ability to stabilize nearby radical sites.[33,61] The star-branched polymer (Figure 2b) also fragments extensively at the junction sites of the PS chains. Three fragment distributions are formed, reflecting the number of detachable arms in the 4-arm star polymer analyzed.

Simple visual inspection of the tandem mass spectra in Figures 1b and 2 allows the straightforward differentiation of the corresponding molecular architectures. Cyclic polymers can similarly be distinguished because they require the breakup of at least two bonds to dissociate, thus leading to more-abundant high-mass and less-abundant low-mass MS^2 products than linear chains (unbranched or branched).[33,59] In all cases, rigorous interpretation of the fragment peaks provides compositional insight that can be used to confirm the exact substituents and linkers incorporated in a polymer and in many cases also to identify unknown polymer structures. Moreover, analogous end-group and architectural information can be obtained for other polymers undergoing homolytic cleavages and radical-induced decompositions upon MS^2, such as poly(methyl acrylate)s and poly(methyl methacrylate)s.[57]

2.2. Polymer Sequences

Tandem mass spectrometry can be used to distinguish isomeric copolymers, to establish copolymer sequences, and to determine copolymer-block sizes. The first two capabilities are documented in Figure 3 by the MS^2 spectra of two PS copolymers that contain one repeat unit with a dimethylsilyl substituent in either the *meta* or the *para* position of the phenyl group. Polymerization was performed using a mixture of the comonomers (namely, styrene and either *m*- or *p*-(dimethylsilyl)styrene),[54] from which various sequences can potentially arise. $[M+Li]^+$ ions were employed for MS^2 analysis, as oxidation of Si–H to Si–OH groups occurs in $[M+Ag]^+$.[63]

The MS^2 spectra of the two copolymers show considerable differences, providing strong evidence that the location of the silylated comonomer in the polymer chain depends on the site of the $Si(CH_3)_2H$ substituent. The spectra are dominated by the a_n and y_n series characteristic for linear polystyrenes which, as mentioned in Section 2.1, contain the α (C_4H_9) or ω (H) chain end, respectively. These fragments partially encompass styrene units only (marked by * and ^ in Figure 3) and partially include the silylated monomer as well (marked by + and & and denoted by $^{Si}a_n$ and $^{Si}y_n$, respectively).

With the *meta* functionalized copolymer (Figure 3a), the silyl group content of the a_n and y_n fragments gradually increases with fragment size; smaller fragments (m/z 400–500) are largely homopolymeric, whereas larger fragments ($m/z > 1000$) are almost exclusively copolymeric (that is, they contain the silylated comonomer). Such a pattern is indicative of random incorporation of the *meta* comonomer into the PS chain.[54] In sharp contrast, the *para* functionalized copolymer (Figure 3b) produces mostly copolymeric a_n but homopolymeric y_n fragments, which indicates incorporation of the *para* silylated monomer near the initiator and not randomly.[54] Hence, MS^2 permits not only differentiation of the sequences produced in the synthesis, but also determination of the preferred comonomer locations along the chain, which reveals insight into the relative comonomer reactivities.

The described strategy requires that the dissociation characteristics of the relevant polymer class (polystyrenes in this case) be known.[33,54] De novo sequencing is generally impossible, unless the polymer has a predesigned sequence, as do peptides and oligonucleotides. Monodisperse polymers with such controlled (encoded) sequences have been recently synthesized on solid resins using established chemoselective reactions.[64–66] For example, poly(alkoxyamine amide)s with specific sequences have been prepared by iteration of two steps, namely the reaction of a primary amine with a Br-

containing anhydride and the coupling of the resulting intermediate with an amino-functionalized nitroxyl radical;[64,66,67] using two different anhydrides and repeating these two steps four times created the binary-coded polymer shown in Figure 4.[67] ESI, followed by MS^2 and de novo interpretation of the observed fragments, allows one to decipher (read) the encoded sequence, as outlined in Figure 4.[64,68,69]

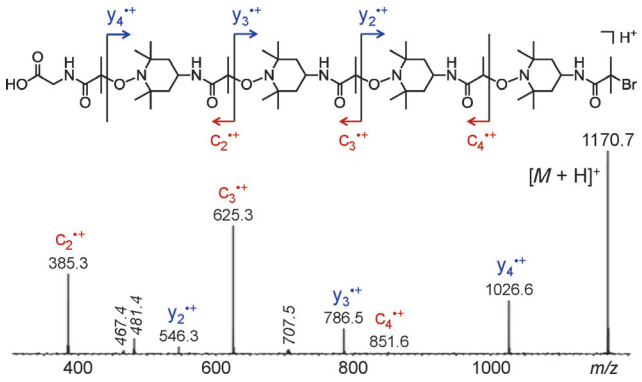

Figure 4. ESI-MS^2 (CAD) spectrum of the $[M+H]^+$ ion from the tetra(alkoxyamine amide) shown on top (m/z 1170.7), acquired using a quadrupole(Q)/ToF mass spectrometer. This oligomer was prepared on a solid amine-functionalized resin using 2-bromoisobutyric anhydride (**1**), 2-bromopropionic anhydride (**0**), and 4-amino-2,2,6,6-tetramethylpiperidine-1-oxyl (**T**) to obtain the putative sequence α-**1**-**T**-**1**-**T**-**1**-**T**-**0**-**T**-**1**-Br, where $\alpha = NHCH_2CO_2H$ is the chain end supplied by the solid support. The expected sequence is confirmed by the observed $c_n^{\bullet+}$ and $y_n^{\bullet+}$ fragment series (italicized m/z values designate internal fragments). Adapted from Ref. [67] with permission.

The copolymers discussed so far contain closely related comonomers, incorporated to enable branching chemistry or to encode digital information. On the other hand, comonomers with substantially different structures and polarities are combined in amphiphilic copolymers, which typically have block architectures.[70,71] The MS^2 characteristics of the latter polymers depend on the fragmentation energetics of their blocks, which can differ considerably depending on the functional groups and connectivity of their repeat units (see Section 2.3).[33,72]

Copolymers comprising hydrophobic polyesters linked with hydrophilic polyethers, which constitute an important class of amphiphiles,[71] fragment extensively within the polyester block if energetically favorable 1,5-H rearrangements can take place at the ester groups.[33] Because this dissociation proceeds at all ester groups in the copolymer, the number of fragments formed helps to determine the corresponding block sizes. This is documented in Figure 5 for a polycarprolactone-*block*-poly(ethylene oxide) copolymer (PCL_m-*b*-PEO_n). The MS^2 spectrum of the lithiated PCL_9-*b*-PEO_7 oligomer includes nine abundant fragments, confirming the presence of nine ester groups (nine PCL units) in this chain, at which the mentioned rearrangement can proceed. The smallest, PCL-free fragment (m/z 329), arising by dissociation at the ester bond joining the PCL and PEO blocks, on the other hand corroborates the PEO_7 block size.

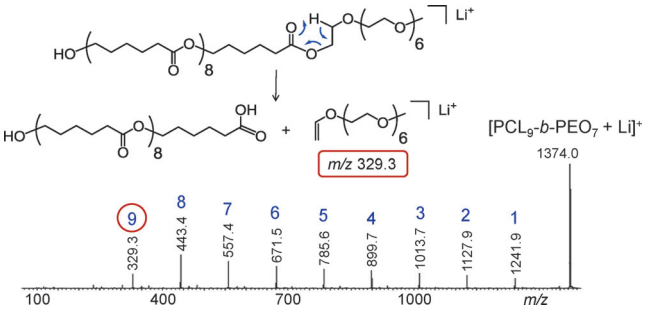

Figure 5. ESI-MS^2 (CAD) spectrum of lithiated PCL_9-*b*-PEO_7 (m/z 1374.0), acquired on a quadrupole ion trap (QIT). All fragments arise from 1,5-H rearrangements at the ester groups; the scheme depicts the reaction occurring at the ester group linking the blocks, which cleaves the entire PCL block. The integers above the peaks indicate the number of repeat units in the PCL chain cleaved to form the observed fragments.

2.3. MS^2 Fragmentation Energetics

The dissociation energies of polymer ions represent an intrinsic structural property; however, their exact values are difficult to determine because of the numerous competitive and consecutive reactions of such large species and the excess energy needed to cause fragmentation within the short residence time of the ions in the mass spectrometer (kinetic shift).[73,74] Information about relative fragmentation energetics can still be gained by energy-resolved MS^2 experiments.[75–78] For this, a polymer ion is subjected to CAD at different collision energies and the survival yield (SY), defined as the intensity of the polymer ion divided by the total ion intensity in the MS^2 (CAD) spectrum, is plotted against the corresponding center-of-mass collision energy (E_{CM}) to construct a SY curve. The use of E_{CM} instead of the laboratory-frame kinetic energy (E_{Lab}) accounts for differences in the mass and number of degrees-of-freedom (DoF) among different *n*-mers. The collision energy corresponding to a SY of 0.5 (50%), namely CE_{50}, provides a parameter that can be used to rank the relative stability of the polymer ion under study.

Figure 6 shows the SY curves for several PCL and PEO oligomers. It is evident from the corresponding CE_{50} values that PCL chains decompose more easily than PEO chains of comparable mass. More importantly, PCL_m-*b*-PEO_n oligomers give rise to SY curves and CE_{50} values that are strikingly similar with those of PCL oligomers, justifying the efficient fragmentation of the copolymer at the PCL block to form fragments that enable facile determination of the PCL block size (see Section 2.2).

An alternative method to assess MS^2 fragmentation energetics is to monitor the polymer-ion intensity as a function of collision energy and select the CE value at which the intensity drops below noise level, namely CE_0, as a representative quantity of the polymer ion's intrinsic stability. This approach, combined with ion-mobility (IM) separation of the MS^2 products, has been termed gradient tandem mass spectrometry (gMS^2);[79,80] it is particularly useful for supramolecular species that dissociate readily without any applied

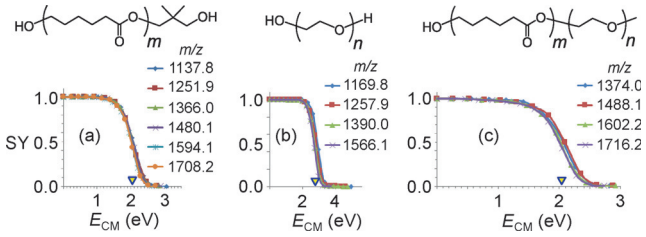

Figure 6. SY curves of $[M+Li]^+$ ions formed by ESI of a) PCL_m, b) PEO_n, and c) PCL_m-*b*-PEO_n oligomers, acquired on a Q/ToF mass spectrometer. Note that different oligomers of the same polymer give essentially the same curve if SY is plotted against E_{CM}, which accounts for mass differences among the *n*-mers. The corresponding CE_{50} values are indicated by ▽.

collision energy, thus precluding the acquisition of useable SY curves. The gMS^2 technique will be discussed in Section 4.

3. Online LC-MS of Polymers

Online LC-MS can be performed using an ambient ionization method, such as ESI or APCI.[22,25,81–87] LC modes that have been coupled with MS detection for synthetic polymer analysis include size-exclusion chromatography (SEC), liquid chromatography under critical conditions (LCCC), and interactive liquid chromatography, also known as liquid adsorption chromatography (LAC).[82,84] These modes can be implemented in both high-performance (HPLC) as well as ultrahigh-performance (UPLC) systems.[84,88,89] UPLC columns utilize smaller stationary-phase particles (sub-2 μm vs. approximately 5 μm in HPLC) and higher pressures to deliver the mobile phase (1000 bar vs. 400 bar in HPLC), which results in improved resolution, sensitivity, and speed of elution as compared to HPLC.[89]

SEC involves entropy-based fractionation according to the hydrodynamic volume, which is proportional to the molecular size.[90] SEC-MS has been used to separate polydisperse polymers into fractions of narrow molecular-weight distribution (MWD), so that their number-average molecular weights (M_n) can be measured by MS to serve as SEC calibrants; this MS-based SEC calibration enables the determination of accurate MWs for polymers with no adequate standards.[81,92–94] Molar masses up to circa 10 kDa (M_n) have been measured by this procedure.[91–93] It should be noted, however, that the lower ESI efficiency of high-mass oligomers can result in underestimation of the MW for polymers with polydispersities (M_w/M_n) above approximately 1.4 and limits the maximum MW that can be investigated.[92,93] Irrespective of such issues, fractionation before MS analysis increases the dynamic range, allowing for the detection of minor products that reveal mechanistic information about new polymerizations.[95]

In LCCC, the entropic and enthalpic terms in the distribution equilibrium between the stationary and mobile phases are equal; as a consequence, all chains with the same repeat unit have identical retention times and are eluted according to their end groups.[84,90,91] With block copolymers, critical conditions can be adjusted for one of the blocks, resulting in fractionation by the size of the other block, which acts as one of the end groups.[84,96–98] The critical conditions are determined by a series of LC experiments using different mobile-phase compositions.[90] This process is laborious, and the critical conditions established by such means may be valid only for short chain lengths (within < 5000 Da).[96] These issues have prevented LCCC-MS from becoming a broadly used analytical technique and limited its applications to very complex end-group distributions that are difficult to derive by other methods.[84,96,98]

Interactive LC exploits the enthalpic interactions of the sample with the stationary versus mobile phase to achieve separation by polarity (that is, chemical functionality) and mass.[84,90] Reverse-phase (RP) LC, which operates with a nonpolar stationary phase and a polar eluent, is the most widely used chromatographic method because of its high reproducibility and broad applicability; it also is most appropriate for coupling LC to MS, as it employs polar solvents that maximize ESI efficiency.[88] RP-LC-MS is an essential analytical tool in biopolymer characterizations[99] but less common in polymer analysis, in which SEC fractionations dominate because they provide a facile route to measure molecular-weight distributions.[90] More recent studies have, however, documented that RP-LC interfaced with MS, instead of the traditionally used UV/Vis or refractive-index detection, is ideally suitable for the separation and identification of mixtures with constituents of different polarity, as encountered in amphiphilic polymers and surfactants.[84–87,100–102] This capability will be demonstrated with a recent UPLC-MS and $LC-MS^2$ study of the sugar-based nonionic surfactant shown in Figure 7a.[87] Such analyses are expected to become more widely employed owing to the growing importance of nonionic amphiphiles in polymer science[103–106] and the increasing availability of mass spectrometers in polymer laboratories.

Sugar-derived surfactants are prepared by attaching PEO_n chains to the saccharide (ethoxylation) and subsequent partial derivatization of the free hydroxy end groups with fatty acid substituents (esterification). During this process, mono- and di-esterified PEO_n chains are coproduced. Depending on the saccharide and fatty acid used, isobaric constituents may be formed. Thus, the ethoxylated methylglucose (PEO_n-glucam) stearates depicted in Figure 7a overlap with PEO_n stearates because the glucam core is isobaric with four ethylene oxide repeat units. For a conclusive characterization of this complex mixture, use of the LC dimension is essential.

RP-LC fractionates the surfactant blend according to the polarity of its constituents (Figure 7b). The least hydrophobic species (PEO and its aggregates) interact marginally with the nonpolar stationary phase and are thus eluted first; they are followed by the esterified oligomers in the order of increasing hydrophobicity, namely monostearates, then distearates, and finally tristearates. Within the mono- and distearates, those containing the glucam core are observed at shorter retention times than their analogues containing only the PEO chains because of the higher polarity imparted by the sugar moiety.

The surfactant products contained in the LC eluates are identified by LC-MS spectra, as illustrated in Figure 8a for the fraction eluting at 6.48 min (Figure 7b). The lowest

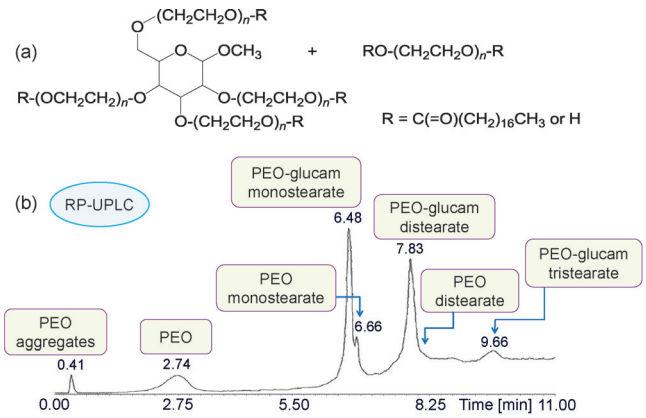

Figure 7. a) PEO_n-glucam stearate prepared by partial esterification of ethoxylated glucam; PEO_n stearates are coproduced in this reaction. b) RP-UPLC-MS chromatogram of the sesquistearate (1.5 mol stearate per mol glucam), acquired on a Q/ToF LC-MS instrument using a C_{18} column and combined isocratic/gradient elution with a two-solvent system (solvent A: 2.55 mM ammonium acetate in water/methanol, 97:3, *v*/*v*; solvent B: methanol). Adapted from Ref. [87] with permission.

chemical noise, highest sensitivity, and highest mass accuracy are achieved using NH_4^+ as the cationization agent, which, unlike the typically used Na^+, minimizes the cogeneration of potassiated and protonated species.[87] Under such conditions, ethoxylated oligomers, including the glucam core, are readily distinguished from isobaric PEO_n chains, based on accurate *m*/*z* measurement. For example, the ion at *m*/*z* 754.502 (Figure 8a) agrees well with the component PEO_{23}-glucam stearate (calculated *m*/*z* 754.506) and is inconsistent with the isobaric component PEO_{27} stearate (calculated *m*/*z* 754.524), confirming the presence of ethoxylated glucam monostearate in the fraction eluting at 6.48 min. Similarly, the LC-MS spectra extracted from all other fractions validate the compositions marked in Figure 7b.

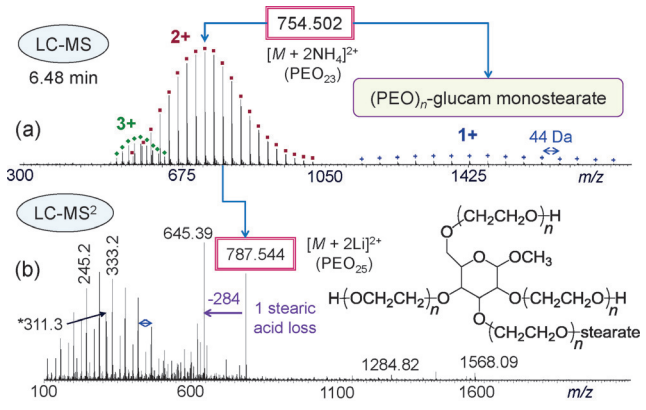

Figure 8. a) LC-MS spectrum of the surfactant fraction eluting at 6.48 min. An ammonium salt was added to the mobile phase as well as post-column to form $[M+xNH_4]^{x+}$ ions ($x=1$–3); their accurate *m*/*z* values reveal that this fraction contains PEO_n-glucam monostearate. b) LC-MS^2 spectrum of the $[M+2Li]^{2+}$ ion from the PEO_{25}-glucam monostearate oligomer in this fraction, obtained by replacing the ammonium salt with a lithium salt. The ester may be attached at any of the PEO chains. Adapted from Ref. [87] with permission.

The fatty acid content in each fraction can additionally be probed by MS^2 experiments by CAD.[86,87] For this, lithiated precursor ions are most suitable because they undergo structurally diagnostic fragmentations at the ester group that release the fatty acid either as a neutral molecule (see Figure 5)[86] or as a dioxolanylium ion;[85] in contrast, ammoniated ions mainly dissociate by NH_3 loss, which does not render useful structural information.[87] Figure 8b depicts the MS^2 spectrum of doubly lithiated PEO_{25}-glucam monostearate. It contains a peak for the stearate dioxolanylium ion, namely $C_{17}H_{35}$-[*cyclo*-$C^+O_2CH_2CH_2$] at *m*/*z* 311.3. Further, a single loss of stearic acid (284 Da) is observed, substantiating the monostearate structure.

Monitoring the fatty acid losses from ethoxylated surfactant cations is particularly useful for oleates, as the unit added upon oleate formation, $C_{18}H_{32}O$, is isobaric with $(C_2H_4O)_6$.[86,107] In this case, the degree of esterification can be simply determined from the number of oleic acid losses observed in the MS^2 spectra.[86]

4. Ion-Mobility Mass Spectrometry

IM-MS[108–110] interfaces mass analysis with ion-mobility spectrometry (IMS),[111] a method in which gas-phase ions are separated by traveling through an electric field in a chamber filled with a bath gas. IMS variants are differentiated according to the type and strength of the electric field and the pressure of the bath gas;[110,111] they include drift tube IMS (DTIMS),[108,109] traveling-wave IMS (TWIMS),[112] trapped-ion mobility spectrometry (TIMS),[113] and field-asymmetric IMS (FAIMS).[114] All of them disperse ions according to their drift times in the IM region, which are determined by the collision cross-section (CCS) and charge state of the ions. The CCS can be viewed as the ions' forward-moving area and reflects both ion size and shape. With IM-MS, ions exiting the IM region pass through a mass analyzer for measurement of their mass-to-charge ratios.[115] Since the IM dimension introduces shape selectivity, it can be used to resolve isomers and isobars with distinct CCS; the more compact structure (that is, the one with the smaller CCS) will drift faster through the IM region, thus arriving earlier at the detector than the more extended or elongated structure. Furthermore, 2D dispersion by CCS and *m*/*z* in the IM and MS dimensions, respectively, deconvolutes chemical noise and separates ions by both charge state and size/shape, thereby increasing the dynamic range and detection sensitivity and facilitating spectral interpretation. These advantages have established IM-MS as an effective analytical tool for the characterization of complex mixtures comprising polymeric isomers,[24,116,117] isobars[86,87,118] or conformers,[119,120] supramolecular assemblies,[26,80,121–125] polymer–polypeptide hybrid materials,[126,127] and polymers differing in architecture[60,128,129] or chirality.[129] In Sections 4.1–4.3, the utility of IM-MS will be illustrated with select studies on supramolecular polymers, hybrid materials, and the thermal desorption/degradation products from nonionizable polymers. All of these studies employed the TWIM variant, in which the IM device is located between the Q and ToF analyzers of a Q/ToF mass spectrometer.

4.1. Snapshots of the Supramolecular Assembly Process

The monomer units of a supramolecular polymer are connected through noncovalent interactions, which are generally weaker than covalent bonds. Such bonding allows supramacromolecules to respond nondestructively to external stimuli, such as temperature or pH changes, but may also lead to the formation of many different architectures during the self-assembly.[130,131] The hierarchical structures evolving in self-assembly reactions can be elucidated by IM-MS and IM-MS^2,[123] as will be shown for π–π bound oligomers formed from a giant amphiphile composed of a perylenetetracarboxdiimide core (PDI) tethered to a hydrophobic polyhedral oligomeric silsesquioxane (POSS) particle and a polar hydroxy or methoxy group at one imide site (POSS-PDI-OR′ with R′ = H or CH_3; see structure in Figure 9).[132] ESI-MS confirms that such amphiphilic substances form polymers (Figure 9); owing to the symmetry of the resulting *n*-mers, however, there is significant overlap of different charge states, each possibly containing more than one isomeric structure. For example, $[M+Na]^+$, $[2M+2Na]^{2+}$, and $[3M+3Na]^{3+}$ from POSS-PDI-OH are superimposed at *m/z* 1327.6 (Figure 9). Mass-selection of this ion and subsequent separation of its components by IMS not only deconvolutes the different charge states but also reveals that $[2M+2Na]^{2+}$ consists of four dimers with distinct drift-time distributions peaking at 2.4, 3.5, 4.3, and 5.5 ms (A–D in Figure 10a). Methylation of

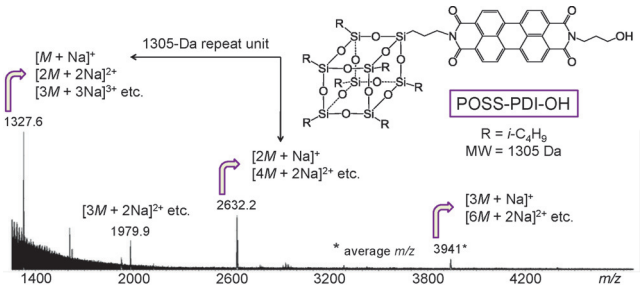

Figure 9. ESI-MS spectrum of POSS-PDI-OH showing self-assembled oligomers (acquired on a Q/ToF mass spectrometer).

the OH group eliminates the fastest (A) and slowest (D) drifting dimer (Figure 10b), providing strong evidence that these complexes include significant hydrogen bonding which is disabled with POSS-PDI-OCH_3. More importantly, the trimer of POSS-PDI-OCH_3 dissociates to yield only one dimer, namely the more compact structure B (Figure 10c).

Supplementary structural information about isomers A–D is gained by their dissociation energetics, assessed by gMS^2.[79] As mentioned in Section 2.3, gMS^2 monitors the peak intensity of IM-separated ions after they have undergone CAD at varying collision energies. The center-of-mass collision energy of disappearance (CE_0) of an ion 's peak is taken as a measure of the intrinsic stability of the ion. The CE_0 values for isomers A–D (Figure 11a) increase in the order $CE_0(A) < CE_0(B) \approx CE_0(C) < CE_0(D)$. This finding, the compactness ranking A < B < C < D (based on the corresponding drift times through the IM region), and the disappearance of

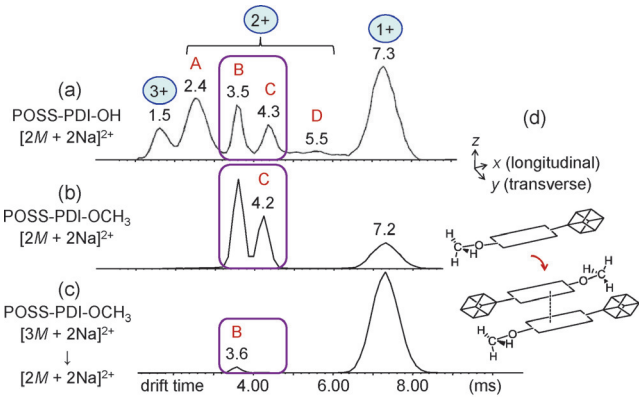

Figure 10. ESI-IM-MS analysis of supramolecular POSS-PDI-OR; IM-MS drift-time distributions of a) $[2M+2Na]^{2+}$ (*m/z* 1327.6) from POSS-PDI-OH, b) $[2M+2Na]^{2+}$ (*m/z* 1342.4) from POSS-PDI-OCH_3, and c) the *m/z* 1342.4 fragment formed by CAD of $[3M+2Na]^{2+}$ (*m/z* 2002.6) from POSS-PDI-OCH_3; d) POSS-PDI-OCH_3 dimer with transversely displaced π–π bonding that allows for further monomer stacking.

structures A and D with POSS-PDI-OCH_3 are reconciled by the conformers depicted in Figure 11b, which involve π–π stacking and hydrogen bonding. Molecular modeling suggests that the optimal π–π overlap is achieved by transverse or longitudinal displacement of the PDI planes (as in B and C, respectively).[133] Longitudinal displacement also enables further stabilization by hydrogen bonding between the hydroxy termini and the carbonyl groups of PDI (D), while hydrogen bonding between the termini (A) significantly lowers the dimer stability because of ineffective π–π overlap. The IM-MS^2 data of Figure 10c indicate that only transverse displacement (structure B) avoids interference between the OR groups and the PDI planes to permit further π–π stacking and 3-mer formation (Figure 10d). Such sampling of the progressive stages of supramolecular assembly provides valuable insight into the nucleation process and the ultimate 3D microstructures of the resulting supramolecular constructs.

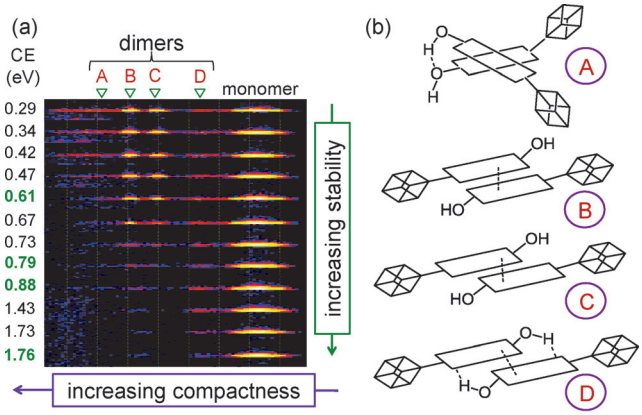

Figure 11. a) gMS^2 spectra of the IM-separated components of $[2M+2Na]^{2+}$ from POSS-PDI-OH (*m/z* 1327.6); the CE_0 values for dimers A, B, C, and D are 0.61, 0.79, 0.88, and 1.76 eV, respectively (in green). b) Dimer structures A–D that account for the compactness and intrinsic-stability trends revealed by the IM-MS data.

4.2. Top-Down Mass Spectrometry of Hybrid Materials

In top-down MS, macromolecular substances are characterized entirely in the mass spectrometer without prior chemical derivatization, degradation, and/or chromatographic purification.[24,80,127] Typically, MS and MS^2 are coupled with a suitable ionization method and IM separation to elucidate the composition and structure of the raw product. Because of the 2D dispersion achieved by the combined MS and IM dimensions, the top-down approach is applicable to mixtures and blends that are difficult to crystallize or purify for analysis by X-ray diffraction or NMR spectroscopy. The top-down procedure will be exemplified with an elastin-mimetic hybrid material composed of hydrophilic poly(acrylic acid) (PAA) blocks attached covalently to blocks of the hydrophobic decapeptide VPGVGVPGVG (VG2).[127] This copolymer was prepared as shown in Scheme 1;[134] telechelic poly(*tert*-butyl acrylate) diazide and the dialkyne-functionalized peptide X(VG2)X (X = *N*-acetylpropargylglycyl at the N-terminus and propargylglycinamide at the C-terminus) were first linked with a click-chemistry reaction (Huisgen [3+2] cycloaddition) to form the hybrid multiblock copolymer $[PtBA\text{-}VG2]_m$. The *tert*-butyl esters were subsequently hydrolyzed to obtain the hybrid material $[PAA\text{-}VG2]_m$, which could contain one or more constituent blocks (m) with linear and/or cyclic architecture, depending on whether the chain ends also underwent a click reaction. Inevitably, this synthetic route generates the desired product in admixture with partially hydrolyzed material and unconsumed reactants.

Using ESI-IM-MS, the product mixture is dispersed by both m/z and size/shape (CCS), which removes chemical noise and separates the desired amphiphilic hybrid according to its charge as well as from unconjugated polymer (PAA and PAA-P*t*BA) and incompletely hydrolyzed hybrid (PAA-P*t*BA-VG2) in various charge states (Figure 12a). Such separation is imperative for reducing spectral congestion and enabling conclusive spectral interpretation.

The compositional assignments given in Figure 12a were deduced from the mass spectra extracted from the IM-separated bands.[127] A representative spectrum, obtained from the mobility region of triply charged PAA-VG2, is depicted in Figure 12b; it contains one series with the PAA repeat unit, arising from triply protonated n-mers with one constituent block, namely $[PAA\text{-}VG2]_1$. Hybrid materials with one constituent block and two proton charges, as well as chains with two constituent blocks and four proton charges are also detected, affirming the synthesis of the desired multiblock copolymer.

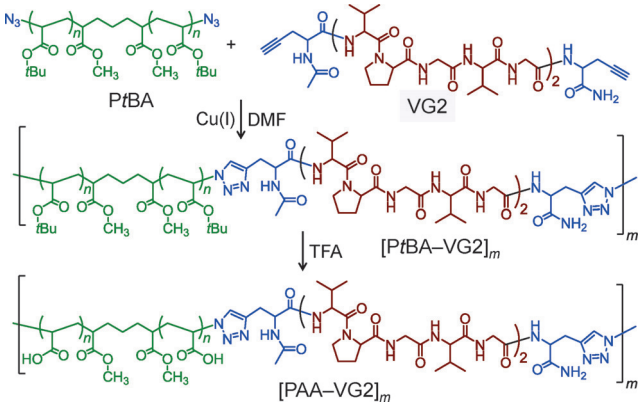

Scheme 1. Synthetic route to hybrid copolymer $[PAA\text{-}VG2]_m$. This product and the intermediate copolymer $[PtBA\text{-}VG2]_m$ can have linear and/or cyclic structures depending on whether the chain ends react to cyclize; only the linear structures are shown for simplicity. Reproduced from Ref. [127] with permission.

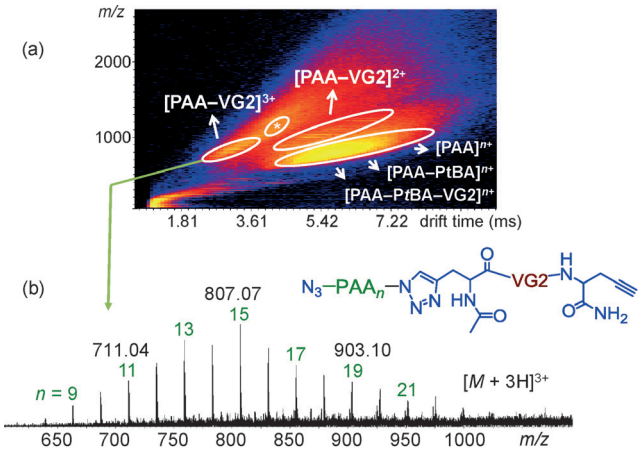

Figure 12. a) ESI-IM-MS plot of the PAA-VG2 hybrid material; the mobility regions of doubly and triply protonated $[PAA\text{-}VG2]_1$ and of incompletely hydrolyzed hybrid as well as unreacted polymer are enclosed in ovals. The region marked with an asterisk contains 4+ ions of $[PAA\text{-}VG2]_2$. b) Mass spectrum extracted from the mobility region of 3+ ions of $[PAA\text{-}VG2]_1$, which could have a linear architecture (shown in the inset) or a macrocyclic architecture if the chain ends react to form a triazole ring. Adapted from Ref. [127] with permission.

The architecture of the hybrid material could be linear or cyclic (see above). This question can be answered by acquiring the collision cross-sections of P*t*BA-VG2 or PAA-VG2 oligomers and comparing them with the theoretical predictions for linear versus cyclic structures. Experimental CCS values are determined from the measured ion-drift times through the IM region (x-axis in Figure 12a); whereas theoretical CCSs are calculated from computationally optimized geometries.[108,127] $[PtBA\text{-}VG2]_1$ n-mers are most suitable for the simulations, as their intramolecular hydrogen-bonding network is markedly simpler than that in $[PAA\text{-}VG2]_1$ n-mers, thus facilitating geometry optimization. The calculated CSS of $[PtBA_n\text{-}VG2+2H]^{2+}$ ions with ten acrylate repeat units ($n=10$) is 464 Å^2 for the cyclic and 499 Å^2 for the linear architecture.[127] The measured CCS for this ion, 468 Å^2,[127] agrees excellently with the value predicted for the cyclic structure, providing strong evidence that all possible [3+2] cycloadditions take place (all-triazole and no alkyne/azide functionalities). This conclusion is corroborated by the CCS data of oligomers with different $PtBA_n$ block lengths ($n=4$, 6, 7, and 8) and for oligomers carrying three H^+ charges.[127]

The foregoing discussion clearly attests that IM drift times and the CCS values derived from them provide an important physical property, characteristic of molecular size and shape,

which can be used to identify and/or differentiate macromolecular architectures. Drift times depend on the potential and drift-gas pressure applied to the IMS region, but CCS values are independent of these parameters and strictly reflect molecular size and shape. Databases of CCS values for a variety of chemical compositions and structures are gradually being created and will certainly improve future elucidations of polymer architectures.

4.3. Top-Down Mass Spectrometry of Cross-Linked or Nonionizable Polymers

Nonionizable polymers, such as polyolefins, and large or cross-linked polymers, such as polyurethanes, rubber copolymers, and hydrogels, cannot be analyzed in intact form by mass spectrometry and also are challenging to characterize directly by other analytical methods. Information about the composition of such materials and their content of additives and stabilizers has traditionally been gained through thermal desorption/degradation, followed by MS analysis of the desorbates and degradants, often after separation by gas chromatography (GC).[135–138] The development of the atmospheric solids analysis probe (ASAP) ionization source,[139] which can be attached to a variety of modern mass spectrometers, including Q/ToF and trap instruments, introduced an alternative means for obtaining useful information about the microstructures of nonionizable, high-molecular-weight, and/or cross-linked materials. The probe contains a heated capillary in which solids or liquids can be deposited for thermal desorption/degradation; the capillary is heated by a stream of nitrogen gas and is located within an APCI source for in situ ionization of the desorption and degradation products. Combining this source with MS, MS^2, and IMS capabilities creates a novel top-down approach for the molecular characterization of the mentioned materials. It is noteworthy that ASAP is operated at relatively low temperatures ($\leq 650\,°C$), yielding not only monomeric molecules but also oligomeric species that provide molecular-connectivity details.

Figure 13a shows the ASAP-IM-MS plot of a commercial polypropylene (PP) sample (pipette tip).[28] The ions formed in the ASAP source can be grouped into three distinct mobility regions after passing through the IMS cell, namely regions 1, 2, and 3. The extracted mass spectra show peaks diagnostic of PP pyrolyzates in region 1 and peaks diagnostic of the stabilizers Irgafos 168 and Irganox 1010 in regions 2 and 3, respectively (Figure 13b). Because of their starlike structures, the stabilizers have more compact architectures than the linear PP pyrolyzates and drift faster through the IM region, thus resulting in adequate separation in the 2D IM-MS plot. Similarly melting PP samples that lack the antioxidants are easily differentiated by the absence of regions 2 and 3 in the ASAP-IM-MS plot.[28]

The ASAP method has been successfully applied to characterize highly fluorinated polymers,[140] blends of biodegradable polyesters with polyethylene,[141] formulated lubricants,[142] insoluble poly(ether ether ketone)s,[143] and grafting on cyclic olefin copolymers.[144] Preliminary data on polyurethane and styrene–butadiene elastomers[29,145] further reveal that ASAP-IM-MS can provide important insight into the composition and additives of industrial thermoplastics, based on which similar products of distinct origin or from different batches can be conclusively identified.[146]

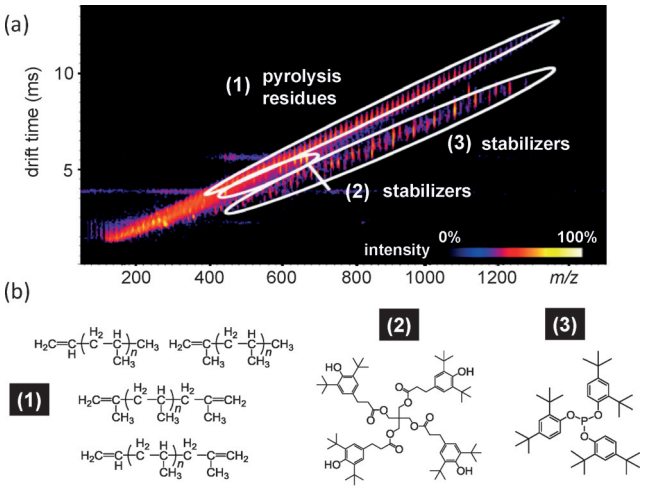

Figure 13. a) ASAP-IM-MS plot of a commercial PP sample and b) compounds identified in the mass spectra extracted from the mobility-separated bands (1), (2), and (3). (All mass spectra contain peaks of molecular radical ions of the compounds shown.) Adapted from Ref. [28] with permission.

5. Outlook

Mass spectrometry is by nature a dispersive technique, probing specific *n*-mers that can be selectively isolated from the sample by their unique mass (literally mass-to-charge ratio, m/z), which unveils elemental-composition information. As a result, MS does not require the high purity necessary for spectroscopic methods of analysis that measure averaged properties, provided that any impurities or byproducts differ in mass from the desired product. On the other hand, a persisting challenge is that pure compounds may give rise to unexpected signals in a 1D mass spectrum because of organic or inorganic impurities in the solvent(s) or matrix (for MALDI) used. In these cases, the LC and/or IM dimensions offer a means to separate such chemical noise, so that the actual sample components can be confidently characterized.

Simple (1D) mass analysis cannot differentiate isomers and variations in sequence or architecture and may not detect certain product components owing to discrimination effects in the ionization event. Again, these problems can be solved by combining MS with orthogonal methods that enable further separation by parameters other than mass, including fragmentation energetics (exploited in the MS^2 dimension), polarity or hydrodynamic-volume differences (utilized in the LC dimension), and/or variations in macromolecular collision cross-sections and charge state (probed by the IM dimension). Using an appropriate combination of these techniques permits the conclusive identification of compositions, end groups, sequences, and 3D architectures for a wide

variety of polymeric materials. Adding mild thermal degradation in the ion source extends the applicability of multidimensional MS to large, cross-linked or not directly ionizable polymers; molecular-weight information is compromised in such cases, but important additive and compositional insight is gained to allow for reverse engineering applications.

The upper mass limit in the multidimensional MS studies described in this Minireview is about 15000 Da for the LC-MS and IM-MS and <5000 Da for the MS^2 experiments; ASAP analyses can be performed with materials of much higher molecular weight, as thermal degradation takes place before MS characterization. Within the mentioned mass limits, oligomer and often isotopic resolution is achieved, which is essential for correct compositional assignments. Future improvements in the resolving power and focusing lenses of ToF and Q/ToF instrumentation[146,147] and the development of sensitive high-mass detectors[148] would certainly increase the MW range amenable to the multidimensional analyses described.

In addition to the approaches discussed in this Minireview, more sophisticated combinations of mass analysis and separation dimensions are possible to tackle more complicated cases. For example, the orthogonal LC and IM separations can be combined to create a 2D separation platform that, when coupled with MS^2 fragmentation, has shown promise in the characterization of pegylated protein drugs.[149] Furthermore, surface-analysis and imaging methods that are widely used in biomedical studies are gradually extended to the synthetic-polymer field.[150–155] These emerging developments and the established methodologies reviewed herein augment the palette of methods available for the microstructure characterization of synthetic (co)polymers, thus significantly facilitating materials research and development.

6. Abbreviations

APCI	atmospheric-pressure chemical ionization
ASAP	atmospheric solids analysis probe
CAD	collisionally activated dissociation
CCS	collision cross-section
CE	collision energy
DTIMS	drift tube ion mobility spectrometry
E_{CM}	center-of-mass collision energy
E_{Lab}	laboratory-frame collision energy
ECD	electron-capture dissociation
ESI	electrospray ionization
ETD	electron-transfer dissociation
FAIMS	field-asymmetric ion mobility spectrometry
gMS^2	gradient tandem mass spectrometry
HPLC	high-performance liquid chromatography
IM-MS	ion-mobility mass spectrometry
IMS	ion mobility spectrometry
LAC	liquid adsorption chromatography
LC	liquid chromatography
LCCC	liquid chromatography under critical conditions
MALDI	matrix-assisted laser desorption ionization
M_n	number-average molecular weight
M_w	weight-average molecular weight
MS	mass spectrometry
MS^2	tandem mass spectrometry
MW	molecular weight
MWD	molecular-weight distribution
PAA	poly(acrylic acid)
PCL	polycaprolactone
PD	photodissociation
PDI	perylenetetracarboxdiimide
PEO	poly(ethylene oxide)
POSS	polyhedral oligomeric silsesquioxane
PP	polypropylene
PS	polystyrene
P*t*BA	poly(*tert*-butyl acrylate)
Q/ToF	quadrupole/time-of-flight
RP-LC	reversed-phase liquid chromatography
SEC	size-exclusion chromatography
SY	survival yield
TIMS	trapped-ion mobility spectrometry
ToF/ToF	tandem/time-of-flight
TWIMS	traveling-wave ion mobility spectrometry
UPLC	ultrahigh-performance liquid chromatography
UV/Vis	ultraviolet-visible spectroscopy
VG2	decapeptide VPGVGVPGVG

Acknowledgements

Financial support from the National Science Foundation (CHE-1308307) is gratefully acknowledged.

How to cite: *Angew. Chem. Int. Ed.* **2017**, *56*, 1452–1464
Angew. Chem. **2017**, *129*, 1474–1487

[1] S. D. Hanton, *Chem. Rev.* **2001**, *101*, 527–569.
[2] *Mass Spectrometry of Polymers* (Eds.: G. Montaudo, R. P. Lattimer), CRC, Boca Raton, **2002**.
[3] H. Pasch, W. Schrepp, *MALDI-TOF Mass Spectrometry of Synthetic Polymers*, Springer, Berlin, **2003**.
[4] *MALDI Mass Spectrometry for Synthetic Polymer Analysis* (Ed.: L. Li), Wiley, Hoboken, **2010**.
[5] *Mass Spectrometry in Polymer Chemistry* (Eds.: C. Barner-Kowollik, T. Gruendling, J. Falkenhagen, S. Weidner), Wiley-VCH, Weinheim, **2012**.
[6] F. Di Girolamo, I. Lante, M. Muraca, L. Putignani, *Curr. Org. Chem.* **2013**, *17*, 2891–2905.
[7] E. Gemperline, C. Keller, L. Li, *Anal. Chem.* **2016**, *88*, 3422–3434.
[8] W. Nie, L. Yan, Y. H. Lee, C. Guha, I. J. Kurland, H. Lu, *Mass Spectrom. Rev.* **2016**, *35*, 331–349.
[9] M. Karas, F. Hillenkamp, *Anal. Chem.* **1988**, *60*, 2299–2301.
[10] K. Tanaka, H. Waki, S. Ido, Y. Akita, Y. Yoshida, T. Yoshida, *Rapid Commun. Mass Spectrom.* **1988**, *2*, 151–153.
[11] J. B. Fenn, M. Mann, C. K. Meng, S. F. Wong, C. M. Whitehouse, *Science* **1989**, *246*, 64–71.
[12] P. Terrier, B. Desmazieres, J. Tortajada, W. Buchmann, *Mass Spectrom. Rev.* **2011**, *30*, 854–874.
[13] C. A. Jackson, W. J. Simonsick, Jr., *Curr. Opin. Solid State Mater. Sci.* **1997**, *2*, 661–667.
[14] M. W. F. Nielen, *Mass Spectrom. Rev.* **1999**, *18*, 309–344.
[15] J. H. Scrivens, A. T. Anthony, *Int. J. Mass Spectrom.* **2000**, *200*, 261–276.

[16] R. Murgasova, D. M. Hercules, *Int. J. Mass Spectrom.* **2003**, *226*, 151 – 162.
[17] P. M. Peacock, C. N. McEwen, *Anal. Chem.* **2004**, *76*, 3417 – 3428.
[18] M. A. Arnould, M. J. Polce, R. P. Quirk, C. Wesdemiotis, *Int. J. Mass Spectrom.* **2004**, *238*, 245 – 255.
[19] G. Montaudo, F. Samperi, M. S. Montaudo, *Prog. Polym. Sci.* **2006**, *31*, 277 – 357.
[20] P. M. Peacock, C. N. McEwen, *Anal. Chem.* **2006**, *78*, 3957 – 3964.
[21] S. M. Weidner, S. Trimpin, *Anal. Chem.* **2008**, *80*, 4349 – 4361; S. M. Weidner, S. Trimpin, *Anal. Chem.* **2010**, *82*, 4811 – 4829.
[22] T. Gruendling, S. Weidner, J. Falkenhagen, C. Barner-Kowollik, *Polym. Chem.* **2010**, *1*, 599 – 617.
[23] G. Hart-Smith, C. Barner-Kowollik, *Macromol. Chem. Phys.* **2010**, *211*, 1507 – 1529.
[24] X. Li, L. Guo, M. Casiano-Maldonado, D. Zhang, C. Wesdemiotis, *Macromolecules* **2011**, *44*, 4555 – 4564.
[25] V. Scionti, B. C. Katzenmeyer, N. S. Erdem, X. Li, C. Wesdemiotis, *Eur. J. Mass Spectrom.* **2012**, *18*, 113 – 137.
[26] Y.-T. Chan, X. Li, J. Yu, G. A. Carri, C. N. Moorefield, G. R. Newkome, C. Wesdemiotis, *J. Am. Chem. Soc.* **2011**, *133*, 11967 – 11976.
[27] X. Shi, S. Gerislioglu, C. Wesdemiotis, *Chromatographia* **2016**, DOI: 10.1007/s10337-016-3077-1.
[28] C. Barrere, F. Maire, C. Afonso, P. Giusti, *Anal. Chem.* **2012**, *84*, 9349 – 9354.
[29] N. Alawani, C. Wesdemiotis, *Proceedings of the 61st ASMS Conference*, Minneapolis, MN, June 9 – 13, **2013**.
[30] A. C. Crecelius, A. Baumgaertel, U. S. Schubert, *J. Mass Spectrom.* **2009**, *44*, 1277 – 1286.
[31] M. J. Polce, C. Wesdemiotis in *MALDI Mass Spectrometry for Synthetic Polymer Analysis* (Ed.: L. Li), Wiley, Hoboken, **2011**, pp. 85 – 127.
[32] V. Scionti, C. Wesdemiotis in *Mass Spectrometry in Polymer Chemistry* (Eds: C. Barner-Kowollik, T. Gruendling, J. Falkenhagen, S. Weidner), Wiley-VCH, Weinheim, **2012**, pp. 57 – 84.
[33] C. Wesdemiotis, N. Solak, M. J. Polce, D. E. Dabney, K. Chaicharoen, B. C. Katzenmeyer, *Mass Spectrom. Rev.* **2011**, *30*, 523 – 559.
[34] L. Sleno, D. A. Volmer, *J. Mass Spectrom.* **2004**, *39*, 1091 – 1112.
[35] T. Yalcin, W. Gabryelski, L. Li, *Anal. Chem.* **2000**, *72*, 3847 – 3852.
[36] A. P. Gies, M. J. Vergne, R. L. Orndorff, D. M. Hercules, *Macromolecules* **2007**, *40*, 7493 – 7504.
[37] M. J. Polce, M. Ocampo, R. P. Quirk, C. Wesdemiotis, *Anal. Chem.* **2008**, *80*, 347 – 354.
[38] M. J. Polce, M. Ocampo, R. P. Quirk, A. M. Leigh, C. Wesdemiotis, *Anal. Chem.* **2008**, *80*, 355 – 362.
[39] A. T. Jackson, A. Bunn, S. Chisholm, *Polymer* **2008**, *49*, 5254 – 5261.
[40] A. P. Gies, S. T. Ellison, M. J. Vergne, R. L. Orndorff, D. Hercules, *Anal. Bioanal. Chem.* **2008**, *392*, 627 – 642.
[41] S. M. Weidner, J. Falkenhagen, K. Knop, A. Thünemann, *Rapid Commun. Mass Spectrom.* **2009**, *23*, 2768 – 2774.
[42] R. Giordanengo, S. Viel, M. Hidalgo, B. Allard-Breton, A. Thevand, L. Charles, *Rapid Commun. Mass Spectrom.* **2010**, *24*, 1941 – 1947.
[43] T. Fouquet, S. Humbel, L. Charles, *J. Am. Soc. Mass Spectrom.* **2011**, *22*, 649 – 658.
[44] A. Nasioudis, R. M. A. Heeren, I. van Doormalen, N. de Wijs-Rot, O. F. van den Brink, *J. Am. Soc. Mass Spectrom.* **2011**, *22*, 837 – 844.
[45] M. Girod, R. Antoine, J. Lemoine, P. Dugourd, L. Charles, *Rapid Commun. Mass Spectrom.* **2011**, *25*, 3259 – 3266.
[46] G. Adamus, W. Sikorska, M. Kowalczuk, I. Noda, M. M. Satkowski, *Rapid Commun. Mass Spectrom.* **2003**, *17*, 2260 – 2266.
[47] P. Rizzarelli, C. Puglisi, G. Montaudo, *Rapid Commun. Mass Spectrom.* **2005**, *19*, 2407 – 2418.
[48] C. Wesdemiotis, F. Pingitore, M. J. Polce, V. M. Russel, Y. Kim, C. M. Kausch, T. H. Connors, R. E. Medsker, R. R. Thomas, *Macromolecules* **2006**, *39*, 8369 – 8378.
[49] P. Terrier, W. Buchmann, B. Desmazières, J. Tortajada, *Anal. Chem.* **2006**, *78*, 1801 – 1806.
[50] G. Adamus, *Rapid Commun. Mass Spectrom.* **2007**, *21*, 2477 – 2490.
[51] M. Girod, T. N. T. Phan, L. Charles, *J. Am. Soc. Mass Spectrom.* **2008**, *19*, 1163 – 1175.
[52] R. Giordanengo, S. Viel, M. Hidalgo, B. Allard-Breton, A. Thevand, L. Charles, *J. Am. Soc. Mass Spectrom.* **2010**, *21*, 1075 – 1085.
[53] T. Fouquet, C. Chendo, V. Toniazzo, D. Ruch, L. Charles, *Rapid Commun. Mass Spectrom.* **2013**, *27*, 88 – 96.
[54] A. M. Yol, J. Janoski, R. P. Quirk, C. Wesdemiotis, *Anal. Chem.* **2014**, *86*, 9576 – 9582.
[55] A. Adhiya, C. Wesdemiotis, *Int. J. Mass Spectrom.* **2002**, *214*, 75 – 88.
[56] K. M. Wollyung, C. Wesdemiotis, A. Nagy, J. P. Kennedy, *J. Polym. Sci. Part A* **2005**, *43*, 946 – 958.
[57] K. Chaicharoen, M. J. Polce, A. Singh, C. Pugh, *Anal. Bioanal. Chem.* **2008**, *392*, 595 – 607.
[58] E. Rivera-Tirado, C. Wesdemiotis, *J. Mass Spectrom.* **2011**, *46*, 876 – 883.
[59] A. M. Yol, D. E. Dabney, S.-F. Wang, B. A. Laurent, M. D. Foster, R. P. Quirk, S. M. Grayson, C. Wesdemiotis, *J. Am. Soc. Mass Spectrom.* **2013**, *24*, 74 – 82.
[60] A. M. Yol, C. Wesdemiotis, *React. Funct. Polym.* **2014**, *80*, 95 – 108.
[61] A. M. Yol, *Determination of Polymer Structures, Sequences, and Architectures by Multidimensional Mass Spectrometry*, Ph.D. Dissertation, The University of Akron, August **2013**.
[62] R. P. Quirk, V. Chavan, J. Janoski, A. Yol, C. Wesdemiotis, *Macromol. Symp.* **2013**, *323*, 51 – 57.
[63] R. P. Quirk, H. Kim, M. J. Polce, C. Wesdemiotis, *Macromolecules* **2005**, *38*, 7895 – 7906.
[64] R. K. Roy, A. Meszynska, C. Laure, L. Charles, C. Verchin, J.-F. Lutz, *Nat. Commun.* **2015**, *6*, 7237. DOI: 10.1038/ncomms8237.
[65] T. T. Trinh, L. Oswald, D. Chan-Seng, L. Charles, J.-F. Lutz, *Chem. Eur. J.* **2015**, *21*, 11961 – 11965.
[66] R. K. Roy, C. Laure, D. Fischer-Krauser, L. Charles, J.-F. Lutz, *Chem. Commun.* **2015**, *51*, 15677 – 15680.
[67] L. Charles, C. Laure, J.-F. Lutz, R. K. Roy, *Macromolecules* **2015**, *48*, 4319 – 4328.
[68] L. Charles, C. Laure, J.-F. Lutz, R. K. Roy, *Rapid Commun. Mass Spectrom.* **2016**, *30*, 22 – 28.
[69] J.-A. Amalian, T. T. Trinh, J.-F. Lutz, L. Charles, *Anal. Chem.* **2016**, *88*, 3715 – 3722.
[70] *Amphiphilic Block Copolymers*: *Self-Assembly and Applications* (Eds.: P. Alexandridis, B. Lindman), Elsevier, Amsterdam, **2000**.
[71] A. B. Kutikov, J. Song, *ACS Biomater. Sci. Eng.* **2015**, *1*, 463 – 480.
[72] A. Nasioudis, N. Memboeuf, R. M. A. Heeren, D. F. Smith, K. Vékey, L. Drahos, O. F. Van den Brink, *Anal. Chem.* **2010**, *82*, 9350 – 9356.
[73] J. Laskin, J. H. Futrell, *Mass Spectrom. Rev.* **2003**, *22*, 158 – 181.
[74] P. B. Armentrout, *J. Am. Soc. Mass Spectrom.* **2013**, *24*, 173 – 185.
[75] F. Rosu, C.-H. Nguyen, E. De Pauw, V. Gabelica, *J. Am. Soc. Mass Spectrom.* **2007**, *18*, 1052 – 1062.

[76] T. M. Kertesz, L. H. Hall, D. W. Hill, D. F. Grant, *J. Am. Soc. Mass Spectrom.* **2009**, *20*, 1759 – 1767.
[77] A. Memboeuf, A. Nasioudis, S. Indelicato, F. Pollreisz, Á. Kuki, S. Kéki, O. F. van den Brink, K. Vékey, L. Drahos, *Anal. Chem.* **2010**, *82*, 2294 – 2302.
[78] D. Smiljanic, C. Wesdemiotis, *Int. J. Mass Spectrom.* **2011**, *304*, 148 – 153.
[79] X. Li, Y.-T. Chan, G. R. Newkome, C. Wesdemiotis, *Anal. Chem.* **2011**, *83*, 1284 – 1290.
[80] K. Guo, Z. Guo, J. M. Ludlow III, T. Xie, S. Liao, G. R. Newkome, C. Wesdemiotis, *Macromol. Rapid Commun.* **2015**, *36*, 1539 – 1552.
[81] D. J. Aaserud, L. Prokai, W. J. Simonsick, Jr., *Anal. Chem.* **1999**, *71*, 4793 – 4799.
[82] R. Murgasova, D. M. Hercules, *Anal. Bioanal. Chem.* **2002**, *373*, 481 – 489.
[83] B. Desmazières, W. Buchmann, P. Terrier, J. Tortajada, *Anal. Chem.* **2008**, *80*, 783 – 792.
[84] J. Falkenhagen, S. Weidner, *Anal. Chem.* **2009**, *81*, 282 – 287.
[85] O. V. Borisov, J. A. Ji, Y. J. Wang, F. Vega, V. T. Ling, *Anal. Chem.* **2011**, *83*, 3934 – 3942.
[86] N. S. Erdem, N. Alawani, C. Wesdemiotis, *Anal. Chim. Acta* **2014**, *808*, 83 – 93.
[87] B. C. Katzenmeyer, S. F. Hague, C. Wesdemiotis, *Anal. Chem.* **2016**, *88*, 851 – 857.
[88] J. C. Arsenault, P. D. McDonald, *Beginners Guide to Liquid Chromatography*, Waters Corporation, Milford, **2009**.
[89] E. S. Grumbach, J. C. Arsenault, D. R. McCabe, *Beginners Guide to UPLC Ultra-Performance Liquid Chromatography*, Waters Corporation, Milford, **2009**.
[90] H. Pasch, B. Trathnigg, *HPLC of Polymers*, Springer, Berlin, **1998**.
[91] M. W. F. Nielen, F. A. Buijtenhuijs, *Anal. Chem.* **1999**, *71*, 1809 – 1814.
[92] X. M. Liu, E. P. Maziarz, D. J. Heiler, G. L. Grobe, *J. Am. Soc. Mass Spectrom.* **2003**, *14*, 195 – 202.
[93] X. M. Liu, E. P. Maziarz, D. J. Heiler, *J. Chromatogr. A* **2004**, *1034*, 125 – 131.
[94] T. Gruendling, M. Guilhaus, C. Barner-Kowollik, *Anal. Chem.* **2008**, *80*, 6915 – 6927.
[95] D. Voll, A. Hufendiek, T. Junkers, C. Barner-Kowollik, *Macromol. Rapid Commun.* **2012**, *33*, 47 – 53.
[96] M. Girod, T. N. T. Phan, L. Charles, *Rapid Commun. Mass Spectrom.* **2008**, *22*, 3767 – 3775.
[97] M. Girod, T. N. T. Phan, L. Charles, *Rapid Commun. Mass Spectrom.* **2009**, *23*, 1476 – 1482.
[98] C. Appiah, K. R. Siefermann, M. Jorewitz, H. Barqawi, W. H. Binder, *RSC Adv.* **2016**, *6*, 6358 – 6367.
[99] W. M. A. Niessen, *Liquid Chromatography-Mass Spectrometry, 3rd ed.*, CRC Press, Taylor & Francis Group, Boca Raton, **2006**.
[100] D. Hewitt, M. Alvarez, K. Robinson, J. Ji, Y. J. Wang, Y.-H. Kao, T. Zhang, *J. Chromatogr. A* **2011**, *1218*, 2138 – 2145.
[101] A. Nasioudis, J. W. van Velde, R. M. A. Heeren, O. F. van den Brink, *J. Chromatogr. A* **2011**, *1218*, 7166 – 7172.
[102] R. Zhang, Y. Wang, L. Tan, H. Y. Zhang, M. Yang, *J. Chromatogr. Sci.* **2012**, *50*, 598 – 607.
[103] R. K. Sharma, *PharmaTutor* **2014**, *2*, 17 – 29.
[104] K. J. M. Bishop, *Angew. Chem. Int. Ed.* **2016**, *55*, 1598 – 1600; *Angew. Chem.* **2016**, *128*, 1626 – 1628.
[105] R. Zolfaghari, A. Fakhru'l-Razi, L. C. Abdullah, S. S. E. H. Elnashaie, A. Pendashteh, *Sep. Purif. Technol.* **2016**, *170*, 377 – 407.
[106] E. M. Pelegri-O'Day, H. D. Maynard, *Acc. Chem. Res.* **2016**, *49*, 1777 – 1785.
[107] J. R. Snelling, C. A. Scarff, J. H. Scrivens, *Anal. Chem.* **2012**, *84*, 6521 – 6529.
[108] M. T. Bowers, P. R. Kemper, G. von Helden, P. A. van Koppen, *Science* **1993**, *260*, 1446 – 1451.
[109] D. E. Clemmer, M. F. Jarrold, *J. Mass Spectrom.* **1997**, *32*, 577 – 592.
[110] A. B. Kanu, P. Dwivedi, M. Tam, L. Matz, H. H. Hill, Jr., *J. Mass Spectrom.* **2008**, *43*, 1 – 22.
[111] G. A. Eiceman, Z. Karpas, H. H. Hill, Jr., *Ion Mobility Spectrometry, 3rd ed.*, CRC, Boca Raton, **2013**.
[112] S. D. Pringle, K. Giles, J. L. Wildgoose, J. P. Williams, S. E. Slade, K. Thalassinos, R. H. Bateman, M. T. Bowers, J. H. Scrivens, *Int. J. Mass Spectrom.* **2007**, *261*, 1 – 12.
[113] K. Michelmann, J. A. Silveira, M. E. Ridgeway, M. A. Park, *J. Am. Soc. Mass Spectrom.* **2015**, *26*, 14 – 24.
[114] B. M. Kolakowski, Z. Mester, *Analyst* **2007**, *132*, 842 – 864.
[115] *Ion Mobility Spectrometry – Mass Spectrometry* (Eds.: C. L. Wilkins, S. Trimpin), CRC, Boca Raton, **2011**.
[116] A. P. Gies, M. Kliman, J. A. McLean, D. M. Hercules, *Macromolecules* **2008**, *41*, 8299 – 8301.
[117] J. N. Hoskins, S. Trimpin, S. M. Grayson, *Macromolecules* **2011**, *44*, 6915 – 6918.
[118] G. R. Hilton, A. T. Jackson, K. Thalassinos, J. H. Scrivens, *Anal. Chem.* **2008**, *80*, 9720 – 9725.
[119] S. Trimpin, M. Plasencia, D. Isailovic, D. E. Clemmer, *Anal. Chem.* **2007**, *79*, 7965 – 7974.
[120] S. Trimpin, D. E. Clemmer, *Anal. Chem.* **2008**, *80*, 9073 – 9083.
[121] Y.-T. Chan, X. Li, M. Soler, J.-L. Wang, C. Wesdemiotis, G. R. Newkome, *J. Am. Chem. Soc.* **2009**, *131*, 16395 – 16397.
[122] E. R. Brocker, S. E. Anderson, B. H. Northrop, P. J. Stang, M. T. Bowers, *J. Am. Chem. Soc.* **2010**, *132*, 13486 – 13494.
[123] X. Li, Y.-T. Chan, M. Casiano-Maldonado, G. A. Carri, G. R. Newkome, C. Wesdemiotis, *Anal. Chem.* **2011**, *83*, 6667 – 6674.
[124] C. A. Scarff, J. R. Snelling, M. M. Knust, C. L. Wilkins, J. H. Scrivens, *J. Am. Chem. Soc.* **2012**, *134*, 9193 – 9198.
[125] M. Wang, C. Wang, X.-Q. Hao, X. Li, T. J. Vaughn, Y.-Y. Zhang, Y. Yu, Z.-Y. Li, M.-P. Song, H.-B. Yang, X. Li, *J. Am. Chem. Soc.* **2014**, *136*, 10499 – 10507.
[126] D. Bagal, H. Zhang, P. D. Schnier, *Anal. Chem.* **2008**, *80*, 2408 – 2418.
[127] A. Alalwiat, S. E. Grieshaber, B. A. Paik, K. L. Kiick, X. Jia, C. Wesdemiotis, *Analyst* **2015**, *140*, 7550 – 7564.
[128] C. D. Foley, D. Casey, B.-Y. Zhang, A. M. Alb, S. Trimpin, S. M. Grayson, *ACS Macro Lett.* **2015**, *4*, 778 – 782.
[129] K. Kim, J. W. Lee, T. Chang, H. I. Kim, *J. Am. Soc. Mass Spectrom.* **2014**, *25*, 1771 – 1779.
[130] J.-M. Lehn, *Polym. Int.* **2002**, *51*, 825 – 829.
[131] H.-J. Schneider, R. M. Strongin, *Acc. Chem. Res.* **2009**, *42*, 1489 – 1500.
[132] B, Sun, W.-B. Zhang, K. Li, C.-L. Wang, X. Ren, S. Yang, Y. Tu, M. Guo, M. Zhu, S. Z. D. Cheng, *Prepr. Symp.-Am. Chem. Soc. Div. Fuel Chem.* **2010**, *55*, 318 – 319.
[133] X. Ren, B. Sun, C.-C. Tsai, Y. Tu, S. Leng, K. Li, Z. Kang, R. M. Van Horn, X. Li, M. Zhu, C. Wesdemiotis, W.-B. Zhang, S. Z. D. Cheng, *J. Phys. Chem. B* **2010**, *114*, 4802 – 4810.
[134] S. E. Grieshaber, B. A. Paik, S. Bai, K. L. Kiick, X. Jia, *Soft Matter* **2013**, *9*, 1589 – 1599.
[135] R. P. Lattimer, *J. Anal. Appl. Pyrolysis* **1993**, *26*, 65 – 92.
[136] M. Blazsó, *J. Anal. Appl. Pyrolysis* **1997**, *39*, 1 – 25.
[137] S. Tsuge, H. Ohtani in *Mass Spectrometry of Polymers* (Eds: G. Montaudo, R. P. Lattimer), CRC, Boca Raton, **2002**, pp. 113 – 147.
[138] S. E. Whitson, G. Erdodi, J. P. Kennedy, R. P. Lattimer, C. Wesdemiotis, *Anal. Chem.* **2008**, *80*, 7778 – 7785.
[139] C. N. McEwen, R. G. McKay, B. S. Larsen, *Anal. Chem.* **2005**, *77*, 7826 – 7831.
[140] C. N. McEwen, H. Major, M. Green, K. Giles, S. Trimpin in *Ion Mobility Spectrometry – Mass Spectrometry* (Eds: C. L. Wilkins, S. Trimpin), CRC, Boca Raton, **2011**, pp. 171 – 197.

[141] C. Barrère, W. Selmi, M. Hubert-Roux, T. Coupin, B. Assumani, C. Afonso, P. Giusti, *Polym. Chem.* **2014**, *5*, 3576 – 3582.
[142] C. Barrère, M. Hubert-Roux, C. Afonso, A. Racaud, *J. Mass Spectrom.* **2014**, *49*, 709 – 715.
[143] E. Cossoul, M. Hubert-Roux, M. Sebban, F. Churlaud, H. Oulyadi, C. Afonso, *Anal. Chim. Acta* **2015**, *856*, 46 – 53.
[144] J. Vieillard, M. Hubert-Roux, F. Brisset, C. Soulignac, F. Fioresi, N. Mofaddel, S. Morin-Grognet, C. Afonso, F. Le Derf, *Langmuir* **2015**, *31*, 13138 – 13144.
[145] N. Alawani, *Structural Characterization of Synthetic Polymers and Copolymers Using Multidimensional Mass Spectrometry Interfaced with Thermal Degradation, Liquid Chromatography and/or Ion Mobility Spectrometry*, Ph.D. Dissertation, The University of Akron, December **2013**.
[146] C. F. Klitzke, Y. E. Corilo, K. Siek, J. Binkley, J. Patrick, M. N. Eberlin, *Energy Fuels* **2012**, *26*, 5787 – 5794.
[147] H. Sato, S. Nakamura, K. Teramoto, T. Sato, *J. Am. Soc. Mass Spectrom.* **2014**, *25*, 1346 – 1355.
[148] F. Chen, S. Gerber, K. Heuser, V. M. Korkhov, C. Lizak, S. Mireku, K. P. Locher, R. Zenobi, *Anal. Chem.* **2013**, *85*, 3483 – 3488.
[149] C. Wesdemiotis, S. Sallam, S. Gerislioglu, B. A. Paik, X. Jia, *Proceedings of the 65th ASMS Conference*, San Antonio, TX, June 4 – 9, **2016**.
[150] S.-F. Wang, X. Li, R. L. Agapov, C. Wesdemiotis, M. D. Foster, *ACS Macro Lett.* **2012**, *1*, 1024 – 1027.
[151] M. Friia, V. Legros, J. Tortajada, W. Buchmann, *J. Mass Spectrom.* **2012**, *47*, 1023 – 1033.
[152] A. D. Celiz, A. L. Hook, D. J. Scurr, D. G. Anderson, R. Langer, M. C. Davies, M. R. Alexander, *Surf. Interface Anal.* **2013**, *45*, 202 – 205.
[153] A. C. Crecelius, J. Vitz, U. S. Schubert, *Anal. Chim. Acta* **2014**, *808*, 10 – 17.
[154] S. J. Gabriel, D. Pfeifer, C. Schwarzinger, U. Panne, S. M. Weidner, *Rapid Commun. Mass Spectrom.* **2014**, *28*, 489 – 498.
[155] P. C. Kooijman, S. J. Kok, J. A. M. Weusten, M. Honing, *Anal. Chim. Acta* **2016**, *919*, 1 – 10.

Manuscript received: July 19, 2016
Revised: October 2, 2016
Accepted Article published: October 6, 2016

